J Nanostruct 12(1): 62-70, Winter 2022

RESEARCH PAPER

Preparation and Deposition the Spinel Ferrite (Cu-$ZnFe_2O_4$) On Al Substrates and Plasticizer Through TP to Study of The Magnetic Characters

Taha Hussein Lazem [1], Rusul Adnan Al-Ward [2], and Nissan Saud [3]*

[1] Directorate General of Education Karkh 3, Ministry of Education, Baghdad, Iraq

[2] Department of Clinical Laboratory Science, College of Pharmacy, Al-Nahrain University, Baghdad, Iraq

[3] Department of Physics, College of Science, Al-Nahrain University, Baghdad, Iraq

ARTICLE INFO

Article History:
Received 14 September 2021
Accepted 29 December 2021
Published 01 January 2022

Keywords:
AFM
SEM
Sol-gel
Thermal evaporation
X-band
X-Ray

ABSTRACT

Technique of sol-gel was utilized to make $Cu_{0.6}Zn_{0.4}Fe_2O_4$ spinel ferrite, then (400 nm and 800 nm) ± 2 0thin films on substrates of Al were precipitated through technique of plasticizer and vacuum as thermal evaporation (TE) through thermal plasma (TP). Tests of diffraction of X-ray (XRD) exposed the thin maked filmsare of polycrystalline nano-structure and the micro-strain occurrence in the crystals because of sintering temperature (ST) influence. Topography images of AFM revealed surfaces as smooth and roughness being low for samples that deposited. Images of surface of SEM thin films present spherical nano-composite grains and the images of cross-sections illustrate agglomerated particles shaped regularly. Influence of thickness on characters of microwave for samples with no any adhesive or fixative addition was revealed and examined through the system of Ne2rk (VNA) Analyzer in X- band width of (8 -12.5) GHz frequency range which illustrates very good stability for the reflectance and very high absorptance proportions.

How to cite this article
Hussein Lazem T, Adnan Al-Ward R, and Saud N. Preparation and Deposition the Spinel Ferrite (Cu-$ZnFe_2O_4$) On Al Substrates and Plasticizer Through TP to Study of The Magnetic Characters. J Nanostruct, 2022; 12(1):62-70. DOI: 10.22052/JNS.2022.01.007

INTRODUCTION

Material characters enactment progress for the previous decades was the crucial aim of several experts [1-11] for evolving such features because of their enormous uses in many sectors of manufactures. Ferrites have been one of such materials that were examined extensively in large [12,13] . Plasmas as thermal (equilibrium) were utilized for processing of material for 100 years and more. One TP mutual example in processing of material is electric welding. Generally, electrical power mostly utilized for igniting plasma is convertion into heat, thus, TPs able to surfaces melting of metallic besides the electrodes utilized for plasma ignition. Nevertheless, it is not desirable to have this extra heat in contact with the softer surfaces or heat-sensitive utilized in processing of material, i.e., cleaning, coating, and etching. For such applications, plasmas being cold might be a worthy substitute, as the e^- are of energy as thermal being high; wherease species as heavier stay "cold". So, generally industrial technology of large-scale is related to non-TPs ignited at low or minimized pressures of gas,

* Corresponding Author Email: dr.rusul.adnan@nahrainuniv.edu.iq

where the temperature of neutral gas is enough low for preventing processing materials damage. Also, there is a history of utilizing plasmas as non-thermal (non-equilibrium) in materials processing; nevertheless, utilizing atmospheric plasmas pressure (APPs) to pereform so is modern. Such approach as innovative to processing of material is appealing as a result of simplicity, less cost, combination and of range of wide possibilities for modification surface and treatment [14,15].

Based on the position of metallic ion, 3 spinel ferrite types are there: spinel ferrite as normal, reverse and random. The parameters of ferrite can be controlled through choosing appropriate synthesis technique along with suitable preparation conditions [12]. Diverse synthesis techniques were utilized to make spinel ferrites, 2 main diverse routes to synthesis a material, conventional ceramic process and non-conventional wet chemical processs include the process as sol-gel [13]. Also, such process is known as the chemical deposition solution process that is widely utilized for the nanomaterials synthesis starting from chemical (sol) solutions named precursors. Precursors mostly are metal alkoxides and chlorides that refer to diverse polycondensation and hydrolysis reactions forms [16]. The formed gel through such process proceeds in lengthy time for drying. Also, it needs high ST (over 1000 °C) for lengthy time to attain phase of purity. The materials as raw, [Zn $(NO_3)_2.6H_2O$, Cu $(NO_3)_2.6H_2O$, Fe $(NO_3)_3.9H_2O$], were chosen with so great purity for avoiding whichever impact on the characters of compound. ($Cu_{1-x}Zn_xFe_2O_4$) formula as ferrite was utilized if X = 0.4 to make the samples $Cu_{0.6}Zn_{0.4}Fe_2O_4$ through a process of sol-gel in which the best findings seemed at such value.

Mathematical formula for the association between the voltage and the current waveforms is resultant from the Telegraphists formulas. A coefficient of reflection ρ or Γ is definite as the ratio of reflected wave to the wave as incident [17]:

$$|\Gamma|^2 = \frac{Power\ reflecte}{Incident\ power} \quad (1)$$

Generally, considering the ne2rk as 2-port, there will be propagating waves into and out of every port. Once there is device linear, the waves of output can be defined in input waves terms as following [18]:

$$b_1 = S_{11}a_1 + S_{12}a_2 \quad (2)$$

$$b_2 = S_{21}a_1 + S_{22}a_2 \quad (3)$$

The parameters of S are constantly dignified in the values as decibel form dB, and for convertion such parameters are in form as (%); one should utilize the formulas 2 and 3 to find [19,20]:

$$\text{Coefficient of reflection } (R\%) = 10^{\left(S11|_{dB}/_{10}\right)}$$

$$\text{Transmission Coefficient } (T\%) = 10^{\left(S21|_{dB}/_{10}\right)}$$

The absorbance % is found through substituting the results of formula 4 and 5 in the formula:

$$A^2 = 1 - R^2 - T^2 \quad (6)$$

and the attenuation reflection or coefficient loss in dB units is measured from the formula:

$$\text{Coefficient of Attenuation} = -20\ Log|S11| \quad (7)$$

The TE process includes evaporating materials source in chamber as vacuumed less than10^{-6} torr and condensation for the particles being evaporated on substrates. In such method, energy as thermal is provided to materials source from where evaporated atoms are for deposited on the substrates. The deposition flux or rate is a travel distance function from the source to the substrates, the impingement angle onto the surface of substrate, the temperature of substrate T.S. and the pressure as base. The thin film ferrite spinel was maked utilizing the «Edward 300» coating system. The evaporation chamber consists of a basic form of cover, heating poles, evaporation boat, substrate holder and vacuum unit [21].

MATERIALS AND METHODS

The sol-gel technique was utilized to make ($Cu_{1-x}Zn_xFe_2O_4$) ferrite[16], in which the amounts of the $C_6H_8O_7$ and NO_3^- measured based on their atomic/MW. The raw material utilized in samples formation were variegated with 80 ml DW in a beaker that was homogenized through stirring as continuous with the model (LMS-1003) as hot plat-stirrers as magnetic.

The solution pH was adjusted to (~7) utilizing solution of ammonia and heating on a hot plate for ½ h at 60 °C. The temperature is increased to 80

ºC with heating as continuous after around 3hrs. Initially, such sol was changed to a gel. Drying was done to the gel was at 120 °C till burntting in a self combustion propagating fashion till all gels were burnt out completely to form a structure that loose fluffy. The material as fluffy was crushed to find ferrite powder utilizing the grinder as electric for 3 min. The ash as as-burnt at 500 °C was calcined for three h to find better homogeneous and crystallization cation distribution in the crystallite as spinel. The powder is variegated with material as glycerin of 6 wt. % with 88% purity as a binder. Attended 2 samples for the ferrite formula (Table 1), and the samples were sintered for 6 hrs at STs 1050 °C with the heating rate 50 °C/min, after that they were lefted to be cooled spontaneously in the furnace inside.

After preparation samples through sol-gel process, thin films was deposited on the Al Al_3 substrates after calculation the mass required to be employed as powder of the ferrite in vaporizer device and after that make the accurate form to get the needed diverse thicknesses with no addition of whichever fixative or adhesive materials [19]. The collected samples inside a cavity were placed for oxidation and moisture prevention, after that inspection the magnetic characters through vector analyzer ne2rk (VNA).

In the current work, the line of Transmission/ Reflection process was utilized to check the microwave maked samples absorbance. Such process includes sample placing in a coaxial or waveguide section line and measuring the 2 parameters as ports complex scattering with a VNA and the calibration should be done prior to measurements preformance. Also, this process includes reflected measurement (S_{11}) and signal as transmitted (S_{21}). The parameters of relevant scattering closely relate to the complex material permeability and permittivity through formulas. The S-parameters conversion to parameter as complex dielectric is computed through solving the formulas utilizing a program. In numerous cases, the process needs preparation the sample i.e., machining as the sample tightly fit into the coaxial or waveguide line [5] 0.1, 0.3, 0.4, 0.5, 0.6 [22]we investigate the possibility of using the heterogeneous materials, with cuboid metallic inclusions inside a dielectric substrate (host. Thin films thickness were measured through estimated wt. process; measured the substrate wt. prior to the deposition of the film, the wt. following film deposition on the substrate, and the difference in wt. (Δm) represents the film wt. Thickness might be achieved utilizing the law of mass [23].

$$t = \frac{\Delta m}{\rho\, d} \tag{8}$$

RESULTS AND DISCUSSION

To investigating the crystal made samples structure following sintering, the analysis of phase was pereformed through system of SHIMADZU XRD-6000 that utilizing radiation of Cu-Kα with 1.54060 A˚ wavelength λ and the range of angles of Braggs are 2θ=5˚- 80˚. XRD analysis is illustraten in Fig. 1 for $Cu_{0.6}Zn_{0.4}Fe_2O_4$ sample that maked at ST 1050 °C with the 0.4 value of x and t= 400 ±20 nm. The findings of this figure illustrating that the structure of the sample is poly-crystalline nature having the cubic thin prepared film phase along acute and peaks as very fine mentioning a worthy crystallization with the chief peak along (311) plane at 2θ =35.461°. The Millar indices (h,k,l) values that diffract for X-ray are (111), (200), (211),

Table (1). The mass samples ratios ($Cu_{1-x}Zn_xFe_2O_4$) made through sol-gel process

Material (g)	Formula of ferrite	
	X = 0.4	$Cu_{0.6}Zn_{0.4}Fe_2O_4$
$Cu(NO_3)2.6H_2O$		102.524
$Zn(NO_3)2.6H_2O$		178.431
$Fe(NO_3)3.9H_2O$		807.712
$C_6H_8O_7.H_2O$		420.281
Total		1508.950

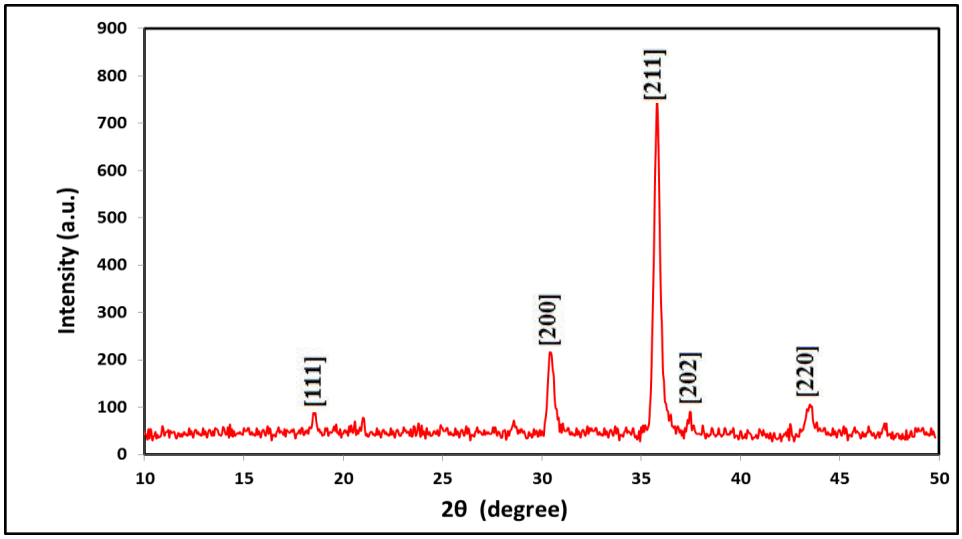

Fig. 1. X-ray pattern of $Cu_{0.6}$ $Zn_{0.6}$ Fe_2O_4 for thickness of 400 ±20 nm at ST 1050 °C.

Table 2. Structure parameters of $Cu_{0.6}Zn_{0.4}Fe_2O_4$ deposited samples on glass for thickness of 400±20 nm and 1050 °C ST

[h k l]	2θº EXP.	d(Å) EXP.	2θº ASTM	d(Å) ASTM	I/I_0	FWHM (deg.)	C.S	MS%
[111]	18.60	4.765	18.508	4.790	6	0.298	27.459	0.509
[200]	30.477	2.930	30.558	2.923	26	0.362	22.109	0.262
[211]	35.808	2.505	35.861	2.502	100	0.362	21.811	0.144
[202]	37.470	2.398	37.121	2.419	6	0.270	57.962	0.868
[220]	43.458	2.080	43.767	2.066	10	0.397	19.405	0.681

(202), (222), and (220) (Fig. 1).

The distance between levels of crystalline (d) was measured through utilizing equation of Bragg [24,25]:

$$\mathrm{d} = \mathrm{a}/\sqrt{h^2 + k^5 + l^2} \quad (9)$$

and the crystallite average size (C.S) estimated utilizing equation of Scherer [24,25]:

$$C.S. = \frac{0.94 \times \lambda}{\Delta\cos(\theta)} \quad (10)$$

In which Δ is width as full at $^1/_2$ maximum in units of radian, λ is the x-ray wavelength (Aº), θ is Braggs diffraction XRD peak angle (degree). The micro strains (M.S) measured from the following [28,29]:

$$\mathrm{M.S} = \left|\frac{\mathrm{a_{ASTM}} - \mathrm{a_{XRD}}}{\mathrm{a_{ASTM}}}\right| \times 100\% \quad (11)$$

The results of XRD are totally matched with the (ASTM) as international standard which presented in Table 2 that indicated to the cubic spinel nano-structure formation.

For investigation the growth quality, grains distribution and Cu-Zn thin roughness films, AFM surface topography 400±20 nm images thickness taken in a mode as contact on a scan sample size (Figure 2). The thin film surface is roughly homogeneous and smooth, microcracks free, holes or pores. Smooth surfaces with roughness being low are essential for the needed physical device applications characters. We measured the roughness average (Ra = 5.3 nm) and thin-film roughness root mean square (Rq = 7.09 nm) from the micrographs of atomic force from the AFM line profiles. The thin film was grown to contain grains of diverse shapes, so the height variation of surface was around 31.2 nm.

SEM of thin film 400±20 nm thickness Cu-Zn

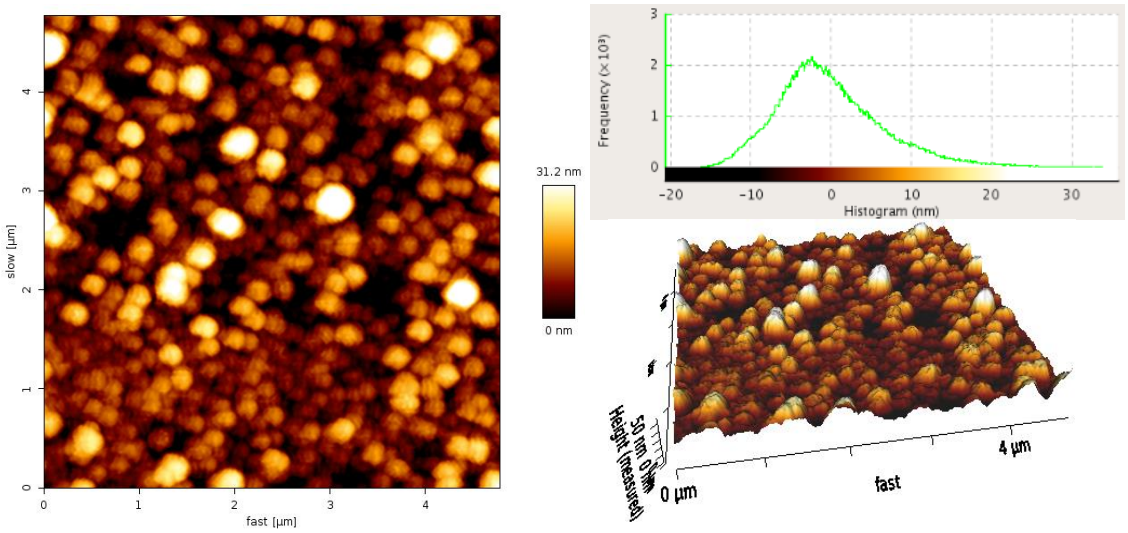

Fig. 2. AFM Cu-Zn ferrite image thin film of 400±20 nm.

ferrite on Al substrate is illustrated in Fig. 3. The micrograph as cross-section illustrats particles, which agglomerated and grown regularly on the substrate. The thin film of Cu-Zn ferrite has enclosed the complete surface of substrate along some random particles overgrowth as proved through the micrographs. From the micrographs of surface, one able to observe that the thin films surface have spherical nano-composite grains of size almost regular and substrates enclosing. It might also be noticed high homogeneousness of surface (such as of good homogeneity) with no defects. The size of grain measured from SEM is found to be of 45.93 nm order that is in good covenant with the size of particle obtained from XRD. The particles growth was related to the surface sintering and diffusion mechanisms at temperatures being high. In the process of sintering, as the temperature elevated, the particles are joined on the surface to each other through mechanism as necking to minimize their surface energy. Such process lasts till the particles are welding to findher[30]–[32]. Thus, the particles surface area and pores are declined throughout the process of sintering.

The microwave absorbance characters of Cu_{1-}

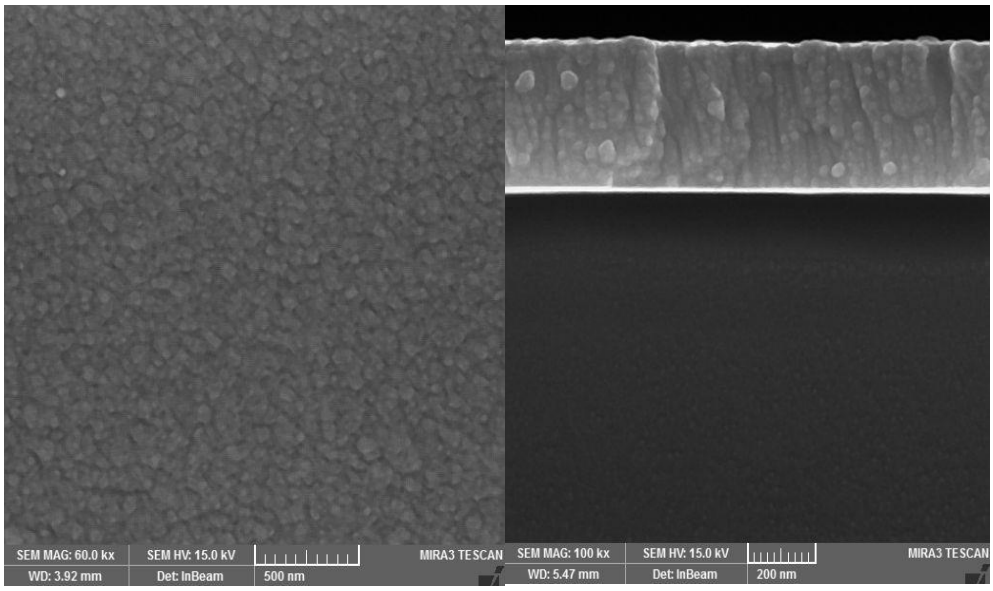

Fig. 3. SEM Cu-Zn ferrite images of thin film 400±20 nm.

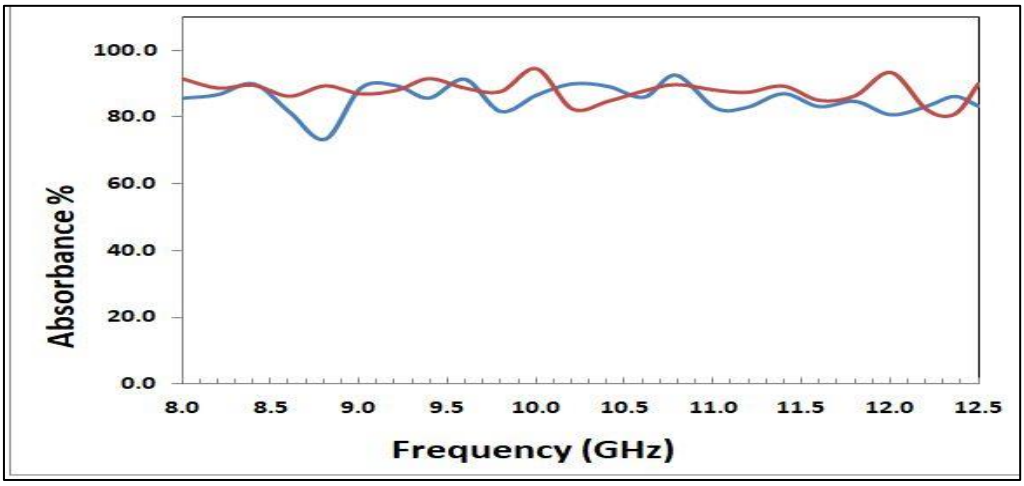

Fig.4. curves of absorbance as a frequency function at range of X-band for samples of $Cu_{0.6}Zn_{0.4}Fe_2O_4$ at 2 diverse thicknesses.

$_xZn_xFe_2O_4$ ferrite samples that made through sol-gel process and in 1050 °C sintered and then placed in TE system vacuum on Al_3 substrates for thicknesses of (400,800) ±20 nm were verified for X-band (8-12.5 GHz) through system of VNA.

Fig. 4 illustrate the absorbance values are very high at 800 nm thickness and the bandwidth being good is (8.40) GHz for region of X- band either bandwidth being good at 800 nm is 9.10 GHz for the range of frequency (8.40-8.61) and (10.21-11.03) GHz, and bandwidth being good at 400 nm is 8.61 GHz for the range frequency (8.20-9.25) and (11.20-11.60) GHz.

Fig. 5 illustrates the coefficient of attenuation as a frequency function. The figure similarities in stability and volatility indicating lack of Zn.

Fig. 6 illustrates the coefficient of reflection as a frequency function to (400 & 800)±20 nm $CuO.6ZnO.4Fe_2O_4$ thickness made samples. Such figure indicated an excellent result of the 2 diverse samples thicknesses if the findings of coefficient of reflection near zero value that means that the reflection is so small. From the figure, 2 peaks of resonance appearance are there at 8.41 GHz that are regarded as not normal, and observed that the coefficient of reflection best values was at 800 nm

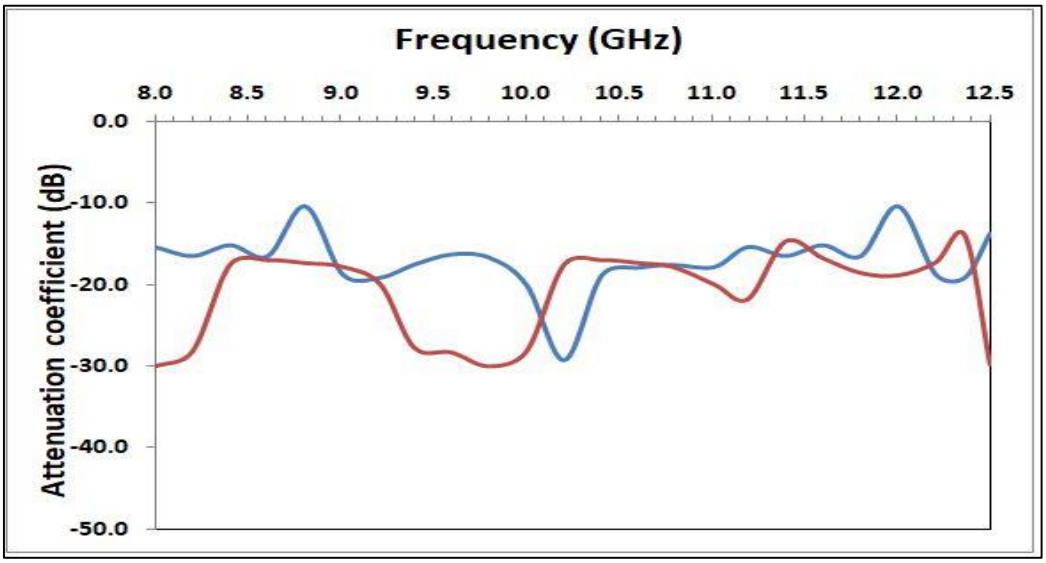

Fig. 5. Coefficient of attenuation as a frequency functions at range of X-band for samples of $Cu_{0.6}Zn_{0.4}Fe_2O_4$ at 2 diverse thicknesses.

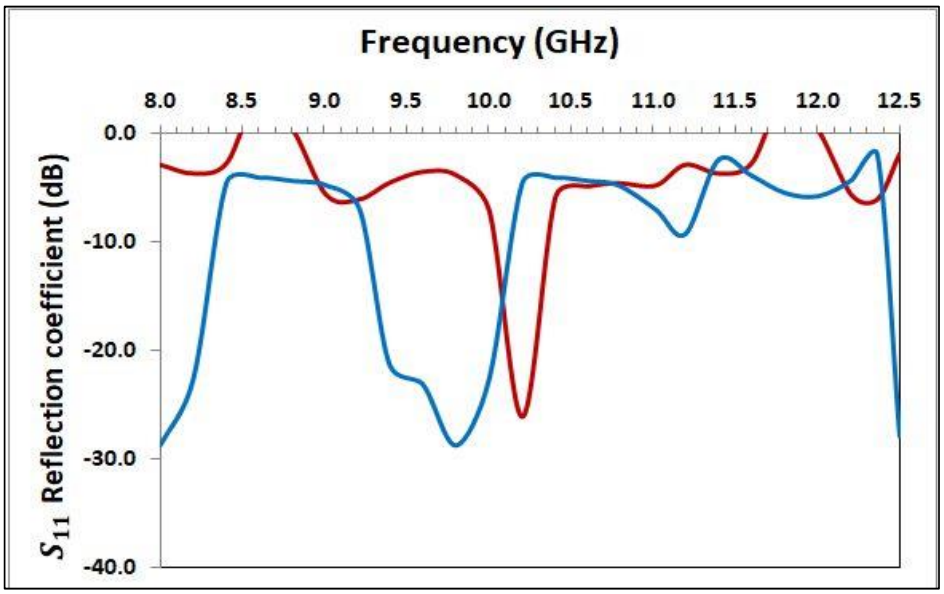

Fig. 6. The coefficient of reflection (S_{11}) as a frequency functions at the range of X-band for samples of $Cu_{0.6}Zn_{0.4}Fe_2O_4$ at 2 diverse thicknesses.

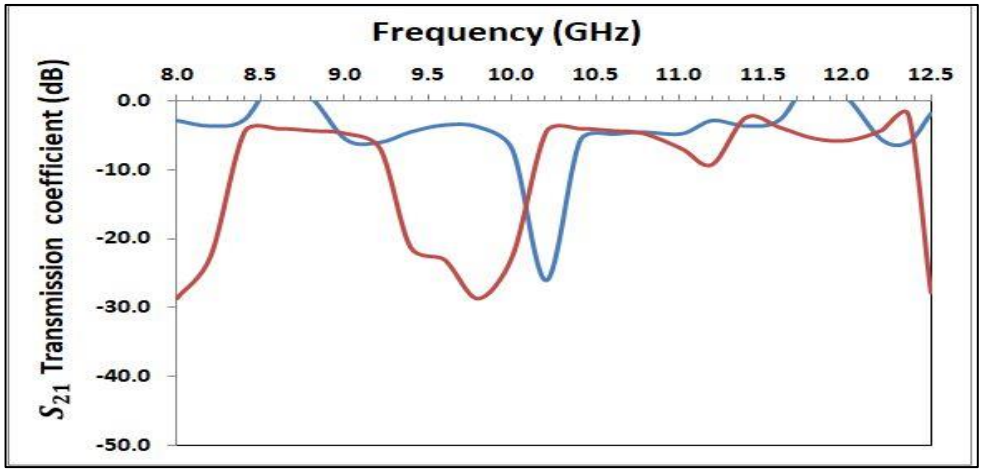

Fig. 7. The transmission coefficient (S_{21}) as a frequency functions at the range of X-band for samples of $Cu_{0.6}Zn_{0.4}Fe_2O_4$ at 2 diverse thicknesses.

because of the ferrite completion, besides because of increased density that minimizes the porosity. The highest coefficient of reflection values at 800 nm are (-7.16, -3.96) dB at frequencies (8.42, 8.66) GHz, correspondingly.

Fig. 7 illustrates that there are transmission coefficient overlap values for the 2 (400 and 800) ±20 nm thicknesses that approves the ferrite development of in 2 thicknesses. One peak of resonance is there for $Cu_{0.6}Zn_{0.4}Fe_2O_4$ 800 nm and 400 nm thicknesses of sample sintered at 1050°C and such peak is formed if there is corresponding in the relative permeability and relative ferrite permittivity. Also we are able to notice that the coefficient of values of attenuation is so good because of the ferrite completion and increased density that minimizes the porosity. The maximum coefficient values of attenuation are (-9.57,-9.89) dB at (9.58, 12.45) GHz frequencies, correspondingly.

CONCLUSIONS

For the currrent work, Cu-Zn ferrite nano-composite thin films were obtained successfully

through the sol-gel process and utilizing the vacuum TE technique to ferrite deposition on Al substrates. XRD- diffraction illustrates a polycrystalline samples structure and the pattern of reflections matching to the planes of (111), (200), (211), (202), and (220) with the chief reflection with (211) plane. Images of AFM expose smooth with low roughness of surface. Images of SEM describe surface of high consistency for the made samples. The samples that deposited offered a good stability and steadier besides, the ferrite absorbance, which deposited on the substrates of Al elevating in higher thickness, while transmission and reflection declining. This work proves the utilizing possibility of thin films spinel ferrite that made through utilizing the sol-gel process with appropriate thickness for devices of microwave, devices of optoelectronic, and many other applications of microwave.

CONFLICT OF INTEREST

The authors declare that there is no conflict of interests regarding the publication of this manuscript.

REFERENCES

1. Hassan MAM, Saleh AF, Mezher SJ. Energy band diagram of In: ZnO/p-Si structures deposited using chemical spray pyrolysis technique. Applied Nanoscience. 2013;4(6):695-701.
2. Hassan MAM, Hateef AA, Majeed AMA, Al-Jabiry AJM, Jameel S, Hussian HARA. Amperometric biosensor of SnO_2 thin film modified by Pd, In and Ag nanostructure synthesized by CSP method. Applied Nanoscience. 2013;4(8):927-934.
3. Mezher SJ, Fadhil RN, Alkhafaji AA, Jasim KA, Shaban AH. The effective of partial replacement of barium by yttrium on $HgBa_{2-x}Y_xCa_2Cu_3O_{8+\delta}$ superconducting compound. TECHNOLOGIES AND MATERIALS FOR RENEWABLE ENERGY, ENVIRONMENT AND SUSTAINABILITY: TMREES19Gr: AIP Publishing; 2019.
4. Hassan ES, Saeed AA, Elttayef AK. Doping and thickness variation influence on the structural and sensing properties of NiO film prepared by RF-magnetron sputtering. Journal of Materials Science: Materials in Electronics. 2015;27(2):1270-1277.
5. Kadhim KJ, Mezher SJ, Yasin NJ, Ismael ZT. Preparation and study magnetic properties of the spinal ferrite $Mg_{1-x}Zn_xFe_2O_4$. Microwave and Optical Technology Letters. 2019;61(7):1741-1746.
6. Mezher SJ, Dawood MO, Beddai AA, Mejbel MK. NiO nanostructure by RF sputtering for gas sensing applications. Materials Technology. 2019;35(1):60-68.
7. Mezher SJ, Kadhim KJ, Abdulmunem OM, Mejbel MK. Microwave properties of Mg–Zn ferrite deposited by the thermal evaporation technique. Vacuum. 2020;173:109114.
8. Aziz WJ, Mezher SJ, Muhsien Hassan MA. Gas sensor of Au/AgNPs/PSi/c-Si using pulsed laser ablation using a YAG:Nd laser. Optik. 2015;126(20):2584-2587.
9. Mezher SJ, Dawood MO, Abdulmunem OM, Mejbel MK. Copper doped nickel oxide gas sensor. Vacuum. 2020;172:109074.
10. Abbas Shah N, Ali A, Ali Z, Maqsood A, Aqili AKS. Properties of Te-rich cadmium telluride thin films fabricated by closed space sublimation technique. J Cryst Growth. 2005;284(3-4):477-485.
11. Mejbel MK, Allawi MK, Oudah MH. EFFECTS OF WC, SiC, IRON AND GLASS FILLERS AND THEIR HIGH PERCENTAGE CONTENT ON ADHESIVE BOND STRENGTH OF AN ALUMINIUM ALLOY BUTT JOINT: AN EXPERIMENTAL STUDY. Journal of Mechanical Engineering Research and Developments. 2019;42(5):224-231.
12. Tatarchuk T, Bououdina M, Macyk W, Shyichuk O, Paliychuk N, Yaremiy I, et al. Structural, Optical, and Magnetic Properties of Zn-Doped $CoFe_2O_4$ Nanoparticles. Nanoscale Research Letters. 2017;12(1).
13. Sattar AA, El-Sayed HM, Agami WR. Physical and Magnetic Properties of Calcium-Substituted Li-Zn Ferrite. J Mater Eng Perform. 2007;16(5):573-577.
14. Penkov OV, Khadem M, Lim W-S, Kim D-E. A review of recent applications of atmospheric pressure plasma jets for materials processing. Journal of Coatings Technology and Research. 2015;12(2):225-235.
15. Kakiuchi H, Ohmi H, Yasutake K. Atmospheric-pressure low-temperature plasma processes for thin film deposition. Journal of Vacuum Science & Technology A: Vacuum, Surfaces, and Films. 2014;32(3):030801.
16. Sutka A, Mezinskis G. Sol-gel auto-combustion synthesis of spinel-type ferrite nanomaterials. Frontiers of Materials Science. 2012;6(2):128-141.
17. Bennett G. P. Basu, Combustion and Gasification in Fluidized Beds, CRC/Taylor & Francis Group, Boca Raton, FL (2006) 491 pp., US$ 129.95, ISBN: 0-8493-3396-2. J Hazard Mater. 2006;138(2):416-416.
18. Microwave Measurements. Institution of Engineering and Technology; 2007.
19. John Wiley and Sons, Inc. IEEE Microwave Magazine. 2010;11(1):35-35.
20. Oscillator Operation and Design Principles. RF and Microwave Transistor Oscillator Design: John Wiley & Sons, Ltd. p. 29-81.
21. Messier R. Thin Film Deposition Processes. MRS Bull. 1988;13(11):18-21.
22. Wu WM, Njoku CC, Whittow WG, Zagoskin AM, Kusmartsev FV, Vardaxoglou JC. Studies of permittivity and permeability of dielectric matrix with cuboid metallic inclusions in different orientations. Journal of Advanced Dielectrics. 2014;04(04):1450032.
23. Jassim SA-J, Zumaila AARA, Al Waly GAA. Influence of substrate temperature on the structural, optical and electrical properties of CdS thin films deposited by thermal evaporation. Results in Physics. 2013;3:173-178.
24. Giannini C, Ladisa M, Altamura D, Siliqi D, Sibillano T, De Caro L. X-ray Diffraction: A Powerful Technique for the Multiple-Length-Scale Structural Analysis of Nanomaterials. Crystals. 2016;6(8):87.
25. Bowen DK, Tanner BK. X-Ray Metrology in Semiconductor Manufacturing: CRC Press; 2018 2018/10/03.
26. Sang S, Liu Z, Tian P, Liu Z, Qu L, Zhang Y. Synthesis of small crystals zeolite NaY. Mater Lett. 2006;60(9-10):1131-1133.

27. Higgins MD. Measurement of crystal size distributions. Am Mineral. 2000;85(9):1105-1116.
28. Wang D, Yuan H, Qiang J. The Microstructure Evolution, Mechanical Properties and Densification Mechanism of TiAl-Based Alloys Prepared by Spark Plasma Sintering. Metals. 2017;7(6):201.
29. Zeng P, Wang K, Falkenstein-Smith RL, Ahn J. EFFECTS OF SINTERING TEMPERATURE ON THE PERFORMANCE OF $SrSc_{0.1}Co_{0.9}O_{3-\delta}$OXYGEN SEMIPERMEABLE MEMBRANE. Brazilian Journal of Chemical Engineering. 2015;32(3):757-765.
30. Sun L, Shao R, Tang L, Chen Z. Synthesis of $ZnFe_2O_4$/ZnO nanocomposites immobilized on graphene with enhanced photocatalytic activity under solar light irradiation. J Alloys Compd. 2013;564:55-62.
31. Li Y, Dai G, Zhou C, Zhang Q, Wan Q, Fu L, et al. Formation and optical properties of ZnO:$ZnFe_2O_4$ superlattice microwires. Nano Research. 2010;3(5):326-338.
32. Woo MA, Kim TW, Kim IY, Hwang S-J. Synthesis and lithium electrode application of ZnO–$ZnFe_2O_4$ nanocomposites and porously assembled ZnFe2O4 nanoparticles. Solid State Ionics. 2011;182(1):91-97.